CHALMERS
UNIVERSITY OF TECHNOLOGY

A Kalman-smoother-based known route energy demand predictor for road vehicles

Downloaded from: https://research.chalmers.se, 2026-11-11 10:27 UTC

Citation for the original published paper (version of record):
Emvin, C., Romano, L., Bruzelius, F. et al (2026). A Kalman-smoother-based known route energy demand predictor for road vehicles. IEEE Transactions on Intelligent Transportation Systems. http://dx.doi.org/10.1109/TITS.2026.3728097

N.B. When citing this work, cite the original published paper.

© 2026 IEEE. Personal use of this material is permitted. Permission from IEEE must be obtained for all other uses, in any current or future media, including reprinting/republishing this material for advertising or promotional purposes, or reuse of any copyrighted component of this work in other works.

(article starts on next page)

This article has been accepted for inclusion in a future issue of this journal. Content is final as presented, with the exception of pagination.

A Kalman-Smoother-Based Known Route Energy Demand Predictor for Road Vehicles

Carl Emvin, Luigi Romano, *Member, IEEE*, Fredrik Bruzelius, Bengt Jacobson, Rickard Andersson, and Pär Johannesson

***Abstract*—The increased demand for electric transportation has brought new challenges, many of which relate to the limited range and long charging time. This may be addressed by providing reliable and accurate residual-range estimates and energy-optimized route selections. Crucially, the performance of such systems is largely determined by the accuracy of the underlying energy demand prediction algorithm. Existing solutions typically predict energy demand but fail to derive the prediction uncertainty, an ever more sought-after quantity. Methods that attempt to provide such a measure often rely on data-driven techniques or computationally intensive Monte Carlo simulations. This paper is therefore set out to provide a dynamic model capable of handling varying operating conditions whilst remaining computationally efficient. By regarding the driver reference speed as a measurement, an observer-like prediction model can be formulated. Building on this principle, a vehicle-independent description is attained, owing to the use of merely exogenous parameters. The observer is realized as a *Cubature Rauch-Tung-Striebel Smoother*, which estimates both the state and the uncertainty, providing qualitative information about expected variation. The algorithm's mean prediction is verified by analyzing the velocity profile, the Kalman gain, and the energy demand, all of which exhibit the expected behavior. Its uncertainty estimate is evaluated against real-world vehicle operation data, which show that the considered uncertainty sources significantly contribute to the energy demand prediction uncertainty. Further improvements in accuracy are expected as more uncertainties are accounted for.**

***Index Terms*—Range estimation, CRTSS, energy demand prediction.**

I. Introduction

FOR more than a century, internal combustion engine vehicles (ICEVs) have been the dominant means of road transportation, but the era of electric vehicles (EVs) is finally approaching. The global EV market has seen an exponential increase in car sales from 1 million to 14 million annually over 6 years (2017-2023) [1], as a consequence of the many legislations enacted by unions and governments. For instance, the Swedish authorities demand a CO_2 reduction of 70% over two decades, from 2010 to 2030 [2] and the EU imposes a emission reduction of newly produced heavy vehicles by 15% from the year 2030 onward, compared against reference CO_2 emissions based on monitoring data in the period 1 July 2019 to 30 June 2021 [3]. At the same time, EVs are now at a point where they largely outperform their ICEV counterparts in terms of response time, max torque, and energy efficiency. For instance, the Volvo HD electric can produce 666 hp compared to the D13 540 hp,[1] making EVs an attractive option for hauliers.

Besides the praise, the impediments of reduced driving range and long charging time have a significant impact on transportation flexibility, excluding EVs from many transport operations. The problem stems from the lack of charging infrastructure, the low power delivery at the connector, and the small battery size. Indeed, technological development of charging infrastructure and batteries appears to be the only logical solution to these issues, provided that EVs are to directly replace ICEVs. But the rate of electrification can also be accelerated if transport operations were tailored to the EVs' strengths using smart utilization strategies. For instance, a mixed fleet planning algorithm was shown to increase the presence of EVs in urban regions [4]. It solved the electric vehicle routing problem (EVRP) using the average specific energy consumption (SEC) model, providing an optimal EV to ICEV mix. Other studies showed that simple energy consumption models, such as the SEC model, were insufficiently accurate to use in the EVRP [5]. Because it enforces a linear dependence between distance and energy consumption, the EVRP collapses to the shortest-distance problem. Instead, more complex and accurate energy consumption models must be adopted to ensure the optimal solution is attained.

In [6], consumption models are divided into factor, macroscopic, and microscopic models based on their complexity and accuracy. There, factor models are described as the most rudimentary models, which include the SEC model. Macroscopic models are slightly more intricate, consider-

Received 16 June 2025; revised 2 April 2026 and 13 July 2026; accepted 5 August 2026. This work was supported by the Utility and Trust of Electric VehicLes (U-FEEL) Project funded by the Swedish Energy Agency under Project P2022-00948. The Associate Editor for this article was B. Chen. *(Corresponding author: Carl Emvin.)*

Carl Emvin, Fredrik Bruzelius, and Bengt Jacobson are with the Vehicle Engineering and Autonomous Systems Division, Mechanical Engineering Department, Chalmers University of Technology, 412 96 Gothenburg, Sweden (e-mail: carl.emvin@chalmers.se; fredrik.bruzelius@chalmers.se; bengt.jacobson@chalmers.se).

Luigi Romano is with the Vehicular Systems Division, Department of Electrical Engineering, Linköping University, 581 83 Linköping, Sweden (e-mail: luigi.romano@liu.se).

Rickard Andersson is with the Powertrain Strategic Development, Volvo Group, 405 08 Gothenburg, Sweden (e-mail: rickard.andersson@volvo.com).

Pär Johannesson is with the RISE Research Institutes of Sweden, 412 58 Gothenburg, Sweden (e-mail: par.johannesson@ri.se).

Digital Object Identifier 10.1109/TITS.2026.3728097

[1] Volvo group, "Specifications for Volvo FH Aero," www.volvotrucks.se/sv-se/trucks/models/volvo-fh-aero/specifications.html

© 2026 The Authors. This work is licensed under a Creative Commons Attribution 4.0 License.
For more information, see https://creativecommons.org/licenses/by/4.0/

This article has been accepted for inclusion in a future issue of this journal. Content is final as presented, with the exception of pagination.

ing holistic characteristics of the mission or road segment, including average velocity, total distance, gross combined weight (GCW), and road type. The models permit fragmentary interpretability whilst remaining simple enough to find heuristic characteristics of large fleets of vehicles. Hence, numerous energy agencies and policymakers have built their own energy-consumption and emissions modeling frameworks, including the Motor vehicle emission simulator (MOVES) [7], the National atmospheric emissions inventory (NAEI) [8], and the Network for transport measures (NTM) [9]. They are useful when investigating large fleets of vehicles, road networks, and longer time horizons, but struggle to account for variations in operating conditions along a transport mission. To limit the computational complexity, most macroscopic models exclusively consider the average vehicle velocity, as the computational complexity for such models typically increases exponentially with the number of parameters [10]. To capture higher frequency effects such as accelerations and decelerations, microscopic models, also referred to as second-by-second models, are required. These models operate with significantly more details, delivering a more accurate consumption prediction. For instance, in [11], a data-driven multi-model fusion algorithm is presented. It combines the model outputs of a *Last absolute shrinkage and selection operator model* (Lasso), an *Orthogonal matching pursuit model* (OMP), and an *elastic net model* (EN). In particular, the algorithm commences each model to predict the energy consumption from a set of parameters: vehicle speed, pedal angles, and powertrain temperatures. But because many of these parameters are unknown to a vehicle in advance, the model becomes incapable of predicting energy consumption in real-world applications. In [12], a *radial bias function neural network* (RBF NN) is employed to estimate the residual range. Although effective in the training domain, these models are challenged by the substantial day-to-day variability inherent to heavy-vehicle transport operations [13]. Such models also struggle to handle different vehicle combinations and drivers, owing to their neural network structure. In contrast, physics-based models leverage vehicle parameters, having the benefit of increased autonomy and modularity. By dividing the energy consumption problem into smaller subproblems, research can progress independently in the modeling of powertrain, motion resistances, and energy demand prediction (EDP). Consequently, improving one of the parts aids the progress of the complete energy consumption model. Additionally, advancements in traction force modeling can reduce energy consumption by improving eco-driving strategies. For instance, [14] presents a joint power and thermal management framework to minimize energy consumption and battery aging. The model demonstrated substantial energy savings, which could have been even further improved with a more accurate traction force model.

Beyond deterministic EDPs, several applications have recently shown interest in EDP uncertainty. For instance in [15], the EDP uncertainty is accounted for to avoid EVRP solutions that result in battery depletion. The paper extends the scope of the EVRP by including chance constraints in the optimization problem. In particular, the conservative probabilistic constraint imposes two important demands on EDPs: modeling and minimization of the second moment. The customary method to accomplish this is to propagate input uncertainties through the inverse-dynamic model using the Monte Carlo Method (MCM). This approach was taken in [16], where the difference between the average speed acquired from the traffic and routing database (TRDB) and a set of logged vehicle speeds is compiled into a histogram, showing signs of bimodality. Samples of that histogram are then repeatedly propagated through the EDP algorithm to attain the segment consumption. The procedure is subsequently repeated for all road segments, and the energy demand error distribution of a transport operation is obtained. The paper concluded that the error distribution of energy demand converges to a normal distribution as the number of road segments goes to infinity, following the central limit theorem (CLT). Unfortunately, the computational complexity of the MCM grows exponentially with the number of uncertain variables, possibly making the algorithm infeasible for systems with many sources of uncertainty. In [17], multiple uncertainty sources are incorporated to assess input-output sensitivity in the inverse-dynamic model. Results show that the most influential input uncertainties are the velocity and GCW. Surprisingly, vehicle parameters, including powertrain efficiency, air drag, and rolling resistance coefficient, proved non-influential concerning uncertainty.

Another approach was taken in [18], which applies a two-scale regression model with prediction uncertainty estimated from FEDAvg-Gaussian weights [19]. Its weights are updated by measurements from all the client vehicles, and in return, the client vehicles can use the server weights when predicting energy demand in the future. The same concept, known as participatory sensing, is also utilized in [20]. The concept is appealing but difficult to execute for heavy vehicle operations due to large variations in operating conditions.

To conclude, applications of EDPs have recently shown increasing interest in the EDP uncertainty, for example within EVRP algorithms. To this day, EDP uncertainty is either estimated using MCM or participatory sensing. But these models remain infeasible for real-time applications, given their high computational complexity or need for extensive log data. To address the shortcomings, this paper presents a novel approach to estimating the first and second moments of energy demand by considering the driver as a measurement in a longitudinal vehicle dynamics-based Kalman observer. The model merely utilizes road and weather information, is fast to compute, and doesn't require vehicle log data. It is first introduced in Section II, where the motion and measurement models are derived and discretized. In Section III, the cubature Kalman smoother algorithm is presented, and the energy consumption is derived from the state, traction force. In Section IV, the observability condition is tested for the observer, and the Kalman gain is studied to better understand the model. In Section V, the accuracy of the observer is tested against vehicle log data and compared against a benchmark model.

II. Models

The longitudinal vehicle motion is at any time governed by the longitudinal force balance, a linear combination of

This article has been accepted for inclusion in a future issue of this journal. Content is final as presented, with the exception of pagination.

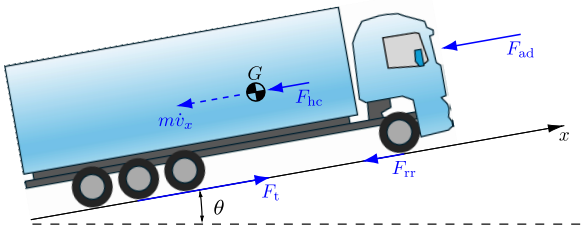

Fig. 1. A free body diagram of a 4×8 rigid truck on a road grade, θ, subject to a rolling resistance force F_{rr}, air drag force F_{ad}, hill climbing force F_{hc}, inertial force $m\dot{v}_x$, and traction force F_t.

the resistive and traction forces. Its details are outlined in Section II-A. In Section II-B, measurement equations and a driver model are introduced, completing the state-space model.

A. Motion Model

The energy consumption of a customary road vehicle, including cars, trucks, and tractors, is most often sufficiently modeled by a point mass subject to motion resistances and a traction force, see Figure 1. The model neglects resistances due to scrubbing, cornering resistance, and suspension losses. Albeit, those generally have a negligible impact on total energy consumption since such conditions are rare and often consume little energy. Neglecting these effects, the governing equation for a point mass model is the linear combination of forces, F_t and F_{mr}, appearing in Newton's law as follows:

$$m\frac{\mathrm{d}v_x}{\mathrm{d}t} = F_t - (F_{rr} + F_{ad} + F_{hc}) = F_t - F_{mr}, \tag{1}$$

where the traction force, F_t, is the force applied at the wheel to propel or brake the vehicle, and F_{mr} is the motion resistance comprised of the rolling resistance force

$$F_{rr} = C_{rr}mg, \tag{2}$$

air drag F_{ad}, and the hill climbing force F_{hc}.

In particular, the rolling resistance is the force opposing vehicle motion resulting from the wheel moment caused by hysteresis in the tire rubber, commonly modeled as a linear relationship between vehicle weight and rolling resistance coefficient, C_{rr}. In [21], the latter is shown to directly depend on tire temperature, T_t, and inflation pressure. The effect is further studied in [22], in which the tire temperature-dependent rolling resistance coefficient is presented,

$$C_{rr} = c_1 + (c_2 - c_1)\mathrm{e}^{-\frac{1}{\lambda}T_t}. \tag{3}$$

In (3), the constant c_1 is the rolling resistance coefficient at high speeds, c_2 is the rolling resistance coefficient at low temperatures ($T_t = 0\ ^\circ C$), and λ is a decay parameter. Noteworthy, the tire temperature, T_t, is the lumped approximation of the distributed state, which has been adopted to simplify the problem. Accordingly, the tire temperature has shown to converge towards a stable temperature, T_t^*, if the operating conditions remain constant, satisfying the ordinary differential equation (ODE),

$$\frac{\mathrm{d}T_t}{\mathrm{d}t} = \frac{T_t - T_t^*}{\tau}, \tag{4}$$

where τ represent the relaxation time. This rolling resistance model fully describes the tire temperature evolution, consequently modeling the rolling resistance coefficient at any time.

Alongside this, the air drag force [23],

$$F_{ad} = \frac{1}{2}\rho A_p C_D \|\boldsymbol{v}_r\|_2^2, \tag{5}$$

is a function of the relative vehicle velocity, $\boldsymbol{v}_r = \boldsymbol{v}_w - \boldsymbol{v}_v$, which is the difference between the vehicle's and the wind's velocity, $\boldsymbol{v}_v$ and $\boldsymbol{v}_w$. The air density can be estimated from the ideal gas law,

$$\rho = \frac{p_d}{R_d T_a} + \frac{p_v}{R_v T_a}, \tag{6}$$

where T_a is the ambient temperature, p_d is the dry air pressure, R_d is the dry air specific gas constant, p_v is the vapor pressure, and R_v is the vapor specific gas constant. The projected area,

$$A_p = A_f \cos\varphi_{aa} + (A_{rs} + A_{ts}) \sin|\varphi_{aa}|, \tag{7}$$

is a function of the rigid truck side area A_{rs}, the trailer side area A_{ts}, the front area A_f, and the attack angle φ_{aa}, which is the angle between the relative vehicle velocity and the longitudinal vehicle axis,

$$\varphi_{aa} = \arccos\frac{-\boldsymbol{v}_v \cdot \boldsymbol{v}_r}{\|\boldsymbol{v}_v\|_2 \|\boldsymbol{v}_r\|_2}. \tag{8}$$

Finally, the air drag coefficient,

$$C_D = C_0 \cos^2\varphi_{aa}, \tag{9}$$

is a function of the nominal air drag coefficient C_0 and the attack angle, φ_{aa}.

The last motion resistance is the hill-climbing force, often referred to as grade resistance. For a road grade, θ, and a GCW, m, the hill-climbing force is given by:

$$F_{hc} = mg \sin\theta. \tag{10}$$

From the governing equation of longitudinal motion, it can be concluded that the minimum state realization is indeed the vector, $\boldsymbol{x} = [v_x\ T_t]^\top$, composed of: vehicle speed and tire temperature, expressed as a function of the independent variable time. Conversely, the road information, presented in the Section II-B, is sampled in the spatial domain. It is hence appropriate to reformulate the motion and tire temperature model using the traveled distance, $s = \int_0^t v_x(t')\,\mathrm{d}t'$, as the independent variable. This is accomplished by applying the chain rule, resulting in the following ODEs:

$$m\frac{\mathrm{d}v_x}{\mathrm{d}s} = \frac{F_t - F_{mr}}{v_x} \tag{11}$$

$$\frac{\mathrm{d}T_t}{\mathrm{d}s} = \frac{T_t - T_t^*}{\tau v_x}. \tag{12}$$

Equations (11) and (12) govern the longitudinal vehicle motion and the evolution of the tire temperature over traveled distance, which is adequate provided that all parameters can be measured precisely and at all instances. Specifically, the model is sensitive to information loss as none of the parameters are described mathematically. By modeling supplementary states, the requirement of the information flow is weaker, and parts of the transport operation, in which parameters are missing, can still be estimated by dead reckoning the model. The supplementary states that could be of interest to model include wind

This article has been accepted for inclusion in a future issue of this journal. Content is final as presented, with the exception of pagination.

velocity and ambient air temperature, as these are considerably uncertain, and road grade, owing to the risk of information loss in construction areas and other unmapped areas. To demonstrate the inclusion of supplementary states whilst alos avoiding to make the collection of ODEs cumbersome, this paper choose to merely model one supplementary state, road grade. This is done using the Langevin equation [24], in which the deterministic representation is the linear ODE,

$$\frac{\mathrm{d}\theta}{\mathrm{d}s} = -\varphi\theta, \tag{13}$$

where θ is the road grade and φ is the damping coefficient. Lastly, the road grade is related to the elevation through the geometric relationship:

$$\frac{\mathrm{d}h}{\mathrm{d}s} = \sin\theta. \tag{14}$$

With the addition of the supplementary states, the state vector, $\boldsymbol{x} = [v_x\ h\ T_\mathrm{t}\ \theta]^\top$, consists of four states, amongst which the most important state, the traction force F_t, is still to be included. Certainly, with the ultimate objective of observing the energy demand, the traction force must be part of the state vector. Indeed, modeling it is difficult, as it depends on the driver, drivetrain, and operating conditions. However, provided that these effects are stationary over a short road segment, the traction force may be formulated as:

$$\frac{\mathrm{d}F_\mathrm{t}}{\mathrm{d}s} = 0. \tag{15}$$

It is important to emphasize that the model is neither a constraint nor the only model contributing to the observed traction force. As will be evident in the coming Sections, the adopted observer framework combines several measurements and models to estimate the traction force. Consequently, all states will vary along the independent variable s under normal operation.

The motion model is now complete, having the states, $\boldsymbol{x} = \begin{bmatrix} v_x & h & T_\mathrm{t} & \theta & F_\mathrm{t} \end{bmatrix}^\top$, and the inputs, $\boldsymbol{u} = \begin{bmatrix} p_\mathrm{a} & T_\mathrm{a} & \boldsymbol{v}_\mathrm{w} & \phi & m \end{bmatrix}^\top$. Out of those, all variables have been introduced except for the vehicle heading angle ϕ. The angle maps the longitudinal vehicle speed onto the global coordinate frame, from which the relative wind velocity can be determined.

Following the establishment of the continuous models, the ultimate objective is to construct an observer, fusing the model predictions with measurements. To proceed with this, the process noise, $\mathbf{B}\boldsymbol{w}$, must be determined to obtain a statistically motivated observer gain. To model this uncertainty, it is helpful to first form two sets of states: the first-order state set, $\boldsymbol{\xi}_1 = \{v_x,\ h\}$, and the second-order state set, $\boldsymbol{\xi}_2 = \{T_\mathrm{t},\ \theta,\ F_\mathrm{t}\}$. The first-order set, $\boldsymbol{\xi}_1$, has the state dynamics described by Newton's second law and the geometric relationship between road grade and elevation. The expectation is thus that the uncertainty of these processes is negligible.

In contrast, the second-order state set, $\boldsymbol{\xi}_2$, is based on approximate relations and shall hence be driven by the process noise, $\mathbf{B}\boldsymbol{w}$. To construct the process noise matrices, the inter-dependencies between the processes must be analyzed. Road grade may be regarded as independent of both tire temperature and traction force, as the vehicle cannot affect the road. Tire temperature, however, is likely influenced by the traction force. Lastly, traction force likely depends on road grade and tire temperature due to their contributions in motion resistances: hill climbing and rolling resistance force. Nevertheless, in contrast to prior rationale, the first approximation, independent noise, is adopted due to difficulties in estimating those interdependencies. The process uncertainty is, after all:

$$\mathbf{B} = \begin{bmatrix} \mathbf{0}_{2,3} \\ \mathbf{I}_3 \end{bmatrix}, \quad \mathrm{Cov}[\boldsymbol{w}] = \mathrm{diag}(\sigma^2_{T_\mathrm{t}},\ \sigma^2_\theta,\ \sigma^2_{F_\mathrm{t}}), \tag{16}$$

where the operator $\mathrm{diag}(\cdot)$ defines the diagonal matrix with the diagonal elements $(\cdot)$.

Building on the equations (1)–(16), five states have been introduced, and their stochastic evolution in space has been presented. From these relations, the non-linear continuous motion model is compiled,

$$\frac{\mathrm{d}\boldsymbol{x}}{\mathrm{d}s} = \boldsymbol{f}(\boldsymbol{x}, \boldsymbol{u}) + \mathbf{B}\boldsymbol{w}, \tag{17}$$

$$\boldsymbol{f}(\boldsymbol{x}, \boldsymbol{u}) = \begin{bmatrix} \frac{F_\mathrm{t} - F_\mathrm{mr}}{m v_x} & \sin\theta & \frac{T_\mathrm{t} - T_\mathrm{t}^*}{\tau v_x} & -\varphi\theta & 0 \end{bmatrix}^\top, \tag{18}$$

where $\boldsymbol{f}(\boldsymbol{x}, \boldsymbol{u})$ models the state inter-dynamics and $\mathbf{B}\boldsymbol{w}$ the uncertainty coupled with each process. Building on the model, a discrete motion model can be obtained by approximating the integral of the continuous motion model using the Euler method, postulating that the state derivatives remain constant over the interval Δs, which can be justified for a short sample distance. By partially applying the Euler method,

$$\boldsymbol{x}_{k+1} \approx \boldsymbol{x}_k + \Delta s \boldsymbol{f}(\boldsymbol{x}_k, \boldsymbol{u}_k) + \int_s^{s+\Delta s} \mathbf{B}\boldsymbol{w}(s')\,\mathrm{d}s', \tag{19}$$

to the deterministic part of the SDE, and saving the integral of the stochastic component, it is possible to express the expected value and covariance without explicitly discretizing it. After all, the last term, $\int_s^{s+\Delta s} \mathbf{B}\boldsymbol{w}(s')\,\mathrm{d}s'$, is a Wiener process, resulting in the first and second moments:

$$\mathbb{E}[\boldsymbol{x}_{k+1}] = \mathbb{E}[\boldsymbol{x}_k] + \Delta s\, \mathbb{E}[\boldsymbol{f}(\boldsymbol{x}_k, \boldsymbol{u}_k)], \tag{20}$$

$$\mathrm{Cov}[\boldsymbol{x}_{k+1} | \boldsymbol{x}_k] = \Delta s \mathbf{B} \mathrm{Cov}[\boldsymbol{w}] \mathbf{B}^\top. \tag{21}$$

B. Measurement Model

Building on the previous Sections, the complete observer requires a measurement model to be introduced. In particular, the model shall facilitate an observable state-space representation. Indeed, for any nonlinear motion model, it is difficult to analyze the criteria for observability. Therefore, at this point, merely the measurement equations are introduced without considering the observability of the system, and an observability analysis is conducted later. Starting with the measurement model for elevation,

$$y_{h,\,k} = h_k + R_{h,\,k}, \quad \text{where } R_{h,\,k} \sim \mathcal{N}(0, \sigma^2_h) \tag{22}$$

where h_k is the state, $y_{h,\,k}$ is the elevation data supplied by the road data supplier, and $R_{h,\,k}$ is the elevation measurement noise, which is very small.

Continuing, the vehicle's longitudinal velocity is measured by a tactical and operational driver [25]. Specifically, the tactical driver produces a set speed, v_d, based on sensory

This article has been accepted for inclusion in a future issue of this journal. Content is final as presented, with the exception of pagination.

information, including legal speed (l), curvature (c), mission stops (m), and traffic control devices (t). In particular, traffic control devices include traffic signals, stop signs, yield signs, and pedestrian crossings, all yielding a zero velocity measurement. The tactical driver is composed of a direct module that evaluates the current situation, and a look-ahead module that assesses future conditions. Starting with the direct module,

$$v_{\mathrm{d}}^{-} = \min(v_{\mathrm{l}}^{-}, v_{\mathrm{c}}^{-}, v_{\mathrm{t}}^{-}, v_{\mathrm{m}}^{-}), \tag{23}$$

which sets the maximum speed permitted, obeying all four speed constraints. The legal speed constraint, v_{l}^{-}, corresponds to the legally permitted speed for the specific vehicle combination, i.e., the maximum speed allowed considering the speed limit and the combination's maximum legal speed.

The second speed constraint regards the road curvature, specifically, the lateral acceleration generated during steady-state driving in a curve. For a point mass model, it is the product of the squared longitudinal vehicle velocity and the curvature C, expressed as the inverse of the curve radius. Hence, assuming the driver wants to avoid lateral accelerations larger than the lateral acceleration limit a_{yl}, the curvature-related speed constraint can be expressed as:

$$v_{\mathrm{c}}^{-} = \sqrt{\frac{a_{\mathrm{yl}}}{C}}. \tag{24}$$

The third speed constraint applies in the event of a traffic control device. The presence of these traffic control devices is relatively rare; hence, it most often does not affect the driver. Nevertheless, when it does, the speed constraint can mathematically be described by the equation:

$$v_{t}^{-} = \begin{cases} 0, & \text{if traffic control device} \\ \infty, & \text{otherwise.} \end{cases} \tag{25}$$

Likewise, the mission stop-related speed constraint, $v_{\mathrm{m}}^{-} = 0$, is only triggered under certain circumstances, characterized by the long stop-time, for instance, during driver rest.

By utilizing the imminent future response from the direct module, $v_{\mathrm{d},\,k+n}^{-}$, the look-ahead module can estimate the maximum current speed that complies with the longitudinal acceleration limit, a_{xl}. Indeed, the permitted vehicle speed given a longitudinal acceleration limit a_{xl}, a target speed $v_{\mathrm{d},\,k+n}^{-}$, and a distance $n\Delta s$ can be expressed using the kinematic relation,

$$v_{\mathrm{d},\,k}^{+} = \sqrt{2n\Delta s a_{\mathrm{xl}} + (v_{\mathrm{d},\,k+n}^{-})^2}, \tag{26}$$

where $n \in \mathbb{N}$ represents the set of unit steps. In essence, the tactical driver finds the probable driver speed by maximizing the current and imminent future speed constraints that are based on exogenous sensory information, available from road maps data suppliers. It should be noted that the reference speed produced by the tactical driver is regarded as a measurement, $y_{v,\,k} \coloneqq v_{\mathrm{d},\,k}^{+}$, taking part in the measurement vector, $y_k = \begin{bmatrix} y_{h,\,k} & y_{v,\,k} \end{bmatrix}^{\top}$, together with the elevation data.

For the reference speed to be useful, a measurement equation relating it to the states is required. This equation is often referred to as the operational driver in dynamic simulation models. An adequate operational driver postulates that the traction force is proportional to the difference between vehicle speed and reference speed, forming the measurement equation,

$$y_{v,\,k} = v_{x,\,k} + \frac{F_{\mathrm{t},\,k}}{K_{\mathrm{p}}} + R_{v,\,k}, \text{ where } R_{v,\,k} \sim \mathcal{N}(0, \sigma_v^2), \tag{27}$$

in which K_{p} represents the proportional gain and $R_{v,\,k}$ the measurement noise characterized by a centered normal distribution. Moreover, the two measurements, reference speed and elevation, are considered to have negligible correlation, hence modeled as jointly independent, $\mathbf{R}_k = \mathrm{diag}(\sigma_{h,\,k}^2,\ \sigma_{v,\,k}^2)$, completing the measurement model.

The use of reference speed as a measurement is indeed unconventional, building on models that describe the driver's response to certain operating conditions as opposed to more conventional vehicle speed measurements, e.g., wheel speed sensor measurements. Unfortunately, the use of said sensor is deemed impossible for an EDP, since the energy demand shall be predicted before the transport operation has started, and hence, no wheel speed sensor measurement can be obtained. Hence, to establish the reference speed as a legitimate measurement, a short segment of a transport operation is analyzed, comparing the logged vehicle speed and the vehicle speed state estimate. Ideally, the measurement $y_{v,\,k}$ is compared against a true signal, $v_{x,\,k} + \frac{F_{\mathrm{t},\,k}}{K_{\mathrm{p}}}$, but it is unfortunately not possible as only positive traction forces are logged by the test vehicle, instead, the state estimate, which is further explained in Section III-A, is used in this comparison. From visual inspection of Figure 2, it can be concluded that the measurement and the state estimate have similar temporal structure, Figure 2a, and distribution of vehicle speed, Figure 2b. Because of unmodeled interference factors such as traffic, transient discrepancies between the measurement and state estimate can be observed in Figure 2a, though its contribution is limited over longer time periods.

III. Estimation Methods

The motion and measurement models presented describe a nonlinear state-space system. To observe the output of this system, a *Cubature Rauch-Tung-Striebel Smoother* (CRTSS) is deployed, and the fundamental equations are presented in Section III-A, along with a discussion on the observer and how its singularities may be avoided. In Section III-B, a method for computing the first and second moments of energy demand is presented.

A. Observer

In general, system dynamics can be estimated using numerous methods, including Kalman and particle filters, as well as smoothers. To make a qualified choice, the state-space model presented in previous Sections is analyzed holistically. Starting with the motion model, which in essence is a nonlinear transformation of states and inputs with additive Gaussian white noise. The set of estimation algorithms can hence be reduced to algorithms supporting non-linear system descriptions.

Moreover, the problem considered in this paper concerns EDPs for specified routes, i.e., the route is known a priori, and the driver follows it. Because road sensory information,

This article has been accepted for inclusion in a future issue of this journal. Content is final as presented, with the exception of pagination.

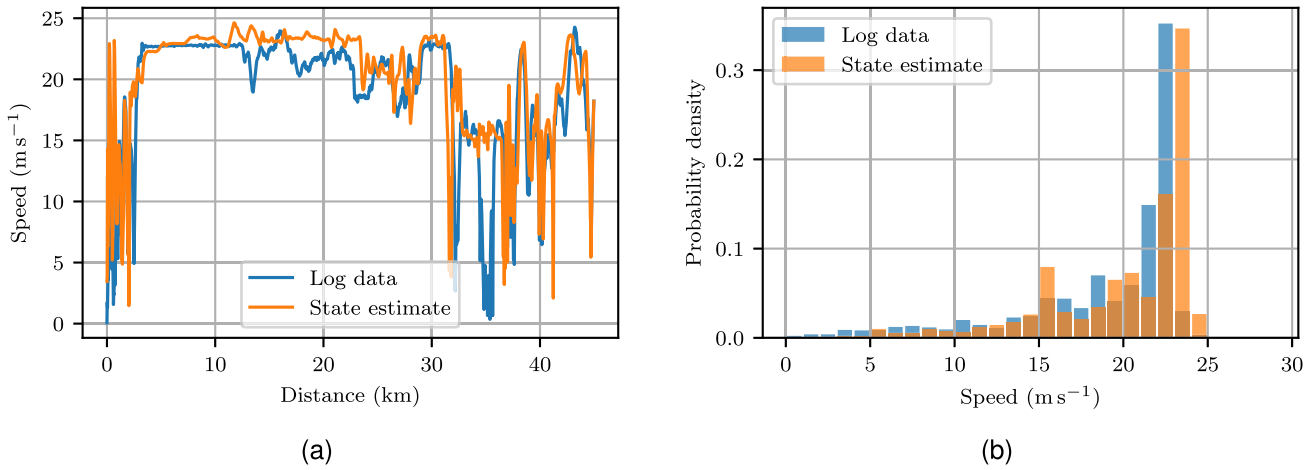

Fig. 2. Figure (a) displays logged vehicle speed (blue) and estimated vehicle speed (orange) over a transport mission. Figure (b) displays the distribution of these speed signals.

including speed limits, curvature, traffic control devices, and altitude profile, is spatially dependent and largely time invariant, it can be acquired before the mission begins. Practical applications of this estimator hence require the driver, haulage, or logistics company to specify the route, and that a mapping between route coordinates and road sensory information is available either onboard the vehicle or through a third-party maps provider.

Likewise, information about the transport mission, including GCW, mission stops, and vehicle configuration details, must also be specified a priori. Indeed, without that information, the accuracy of a heavy vehicle EDP is drastically reduced, especially considering vehicle combinations with a permitted GCW of about 60 metric tonnes. The mission information is hence assumed to be available, either from the driver, haulage, or the logistics company.

Lastly, the weather information is both spatial and time-dependent, complicating the information flow, as the input becomes state-dependent, in this case, time. However, provided that the time can be estimated with reasonable accuracy, the weather information can be acquired from weather forecasts, permitting the use of the information in advance. Hence, all information required by the state-space model: road, mission, and weather, is available before the operation, allowing the use of a smoothing algorithm. The decision between the many smoothing algorithms, including Kalman and particle smoothers, shall be guided by the intended use case and accuracy requirements set by the application. For EDPs, one of the use cases is online estimation in vehicles, requiring a computationally light method. Owing to these considerations, CRTSS appears to be the best choice. It is composed of a two-step process, the forward and the backward pass [26].

Starting with the forward pass, the objective is to predict the state, covariance, and cross-covariance using the cubature moment matching technique. Specifically, it involves transforming strategically placed sigma points through the nonlinear function $\mathbf{f}(\boldsymbol{\chi})$ and subsequently approximating the moments of the function output, building on the same fundamental principle, sample propagation, as the MCM. In contrast to the MCM, the number of samples used in the cubature moment matching algorithm is 2 times the number of states n, which for this particular implementation means 10 sigma points. In particular, the algorithm imposes the following selection of sigma points [26]:

$$\boldsymbol{\chi}_{k-1}^{(i)} = \boldsymbol{x}_{k-1} \pm \sqrt{n}\mathbf{L}^{(i)}, \text{ where } \mathbf{P}_{k-1} = \mathbf{L}\mathbf{L}^T, \tag{28}$$

where $\boldsymbol{x}_{k-1}$ is the state estimate, $\mathbf{P}_{k-1}$ is the covariance matrix, and $\mathbf{L}^{(i)}$ is the i:th column of the Cholesky decomposition. Subsequently, the sigma points are transformed through the motion model and the predicted mean $\boldsymbol{x}_{k|k-1}$, covariance $\mathbf{P}_{k|k-1}$, and cross covariance $\mathbf{D}_{k|k-1}$ are computed as [26]:

$$\boldsymbol{x}_{k|k-1} = \frac{1}{2n}\sum_{i}^{2n} \boldsymbol{f}(\boldsymbol{\chi}_{k-1|k-1}^{(i)}), \tag{29}$$

$$\mathbf{P}_{k|k-1} = \frac{1}{2n}\sum_{i}^{2n} (\boldsymbol{f}(\boldsymbol{\chi}_{k-1}^{(i)}) - \boldsymbol{x}_{k|k-1})(\cdot)^\top + \mathbf{Q}_{k-1}, \tag{30}$$

$$\mathbf{D}_{k} = \frac{1}{2n}\sum_{i}^{2n} (\boldsymbol{\chi}_{k-1}^{(i)} - \boldsymbol{x}_{k-1})(\boldsymbol{f}(\boldsymbol{\chi}_{k-1}^{(i)}) - \boldsymbol{x}_{k|k-1})^\top. \tag{31}$$

Indeed, for the algorithm to work effectively, a new estimate $\boldsymbol{x}_{k-1}$ and $\mathbf{P}_{k-1}$ must be acquired at all unit steps k. To facilitate that, the prediction is updated utilizing a similar procedure as the prediction, starting by generating $2n$ sigma points, this time utilizing the predicted mean and covariance. Thereafter, the sigma points are transformed through the measurement model, and finally, the moments are computed [26]:

$$\boldsymbol{\mu}_{k} = \frac{1}{2n}\sum_{i}^{2n} \boldsymbol{h}(\boldsymbol{\chi}_{k|k-1}^{(i)}), \tag{32}$$

$$\mathbf{S}_{k} = \frac{1}{2n}\sum_{i}^{2n} (\boldsymbol{h}(\boldsymbol{\chi}_{k|k-1}^{(i)}) - \boldsymbol{\mu}_{k})(\cdot)^\top + \mathbf{R}_{k}, \tag{33}$$

$$\mathbf{C}_{k} = \frac{1}{2n}\sum_{i}^{2n} (\boldsymbol{f}(\boldsymbol{\chi}_{k-1}^{(i)}) - \boldsymbol{x}_{k|k-1})(\boldsymbol{h}(\boldsymbol{\chi}_{k|k-1}^{(i)}) - \boldsymbol{\mu}_{k}), \tag{34}$$

$$\mathbf{K}_{k} = \mathbf{C}_{k}\mathbf{S}_{k}^{-1}, \tag{35}$$

This article has been accepted for inclusion in a future issue of this journal. Content is final as presented, with the exception of pagination.

$$\boldsymbol{x}_k = \boldsymbol{x}_{k|k-1} + \mathbf{K}_k(y_k - \boldsymbol{\mu}_k), \tag{36}$$
$$\mathbf{P}_k = \mathbf{P}_{k|k-1} - \mathbf{K}_k\mathbf{S}_k\mathbf{K}_k^\top. \tag{37}$$

The algorithm presented to this end is equivalent to the cubature Kalman filter (CKF) algorithm. The difference between the filter and the smoother resides in the backward pass. By utilizing future measurements, y_{k+T}, and the forward pass predictions, the smoothened estimates may be computed as [26]:

$$\mathbf{G}_{k-1} = \mathbf{D}_{k|k-1}\mathbf{P}_{k|k-1}^{-1}, \tag{38}$$
$$\hat{\boldsymbol{x}}_{k-1} = \boldsymbol{x}_{k-1} + \mathbf{G}_{k-1}(\hat{\boldsymbol{x}}_k - \boldsymbol{x}_{k|k-1}), \tag{39}$$
$$\hat{\mathbf{P}}_{k-1} = \mathbf{P}_{k-1} + \mathbf{G}_{k-1}(\hat{\mathbf{P}}_k - \mathbf{P}_{k|k-1})\mathbf{G}_{k-1}^\top. \tag{40}$$

The observer outlined has significant computational advantages over the MCM, as its computational power demand scales linearly with the number of states. For this problem, a regular laptop with a 12th Gen Intel Core i5 processor can compute the energy demand at a rate of about 40 km/s^{-1}, which corresponds to approximately 3600 times real time. It shall be noted that a significantly faster algorithm may be attained if the backward pass is omitted, the Kalman gain is held constant, and a larger step size is used.

B. Energy Consumption Estimation and Analysis

With the model presented thus far, the first and second moments of energy consumption can be computed analytically. To this end, the consumed energy,

$$E_\mathrm{c}(s) = \int_0^s \frac{F_\mathrm{p}(s')}{\eta_\mathrm{p}}\,\mathrm{d}s', \tag{41}$$

is the spatial-integral of propulsion force, F_p, times the inverse of the powertrain efficiency, η_p. In (41), the propulsion force is derived under the assumption of mutually exclusive brake and propulsion pedals, i.e., the pedal arbitration function:

$$F_\mathrm{p} = \max(F_\mathrm{t}, 0), \quad F_\mathrm{b} = \max(-F_\mathrm{t}, 0). \tag{42}$$

Building on this foundation, the first and second moments of the energy consumption estimate, $\hat{E}_\mathrm{c}$, can be computed using the traction force state estimate, $\hat{F}_\mathrm{t}$, with mean, F_t, and variance, σ_t^2. Without acknowledging the characteristics of the traction force estimate, the propulsion force estimate, $\hat{F}_\mathrm{p}$, can also be expressed as a stochastic variable,

$$\hat{F}_{\mathrm{p},\,k} = F_{\mathrm{p},\,k} + r_k, \tag{43}$$

with mean, $F_{\mathrm{p},k}$, and variance, $\mathbb{E}[r_k^2] = \sigma_{\mathrm{p},\,k}^2$. On this basis, the consumed energy is approximated by the discret integral:

$$\hat{E}_{\mathrm{c},\,k} = \Delta s \sum_{i=1}^{k} \hat{F}_{\mathrm{p},\,i}\eta_{\mathrm{p},\,i}^{-1} = \Delta s \sum_{i=1}^{k}(F_{\mathrm{p},\,i} + r_i)\eta_{\mathrm{p},\,i}^{-1} \tag{44}$$
$$= E_{\mathrm{c},\,k} + \Delta s \sum_{i=1}^{k} r_i\eta_{\mathrm{p},\,i}^{-1}. \tag{45}$$

Moreover, under the assumption that the propulsion efficiency, η_p, and stochastic error variable, r_k, are uncorrelated and time independent, it is possible to find the first and second moments as:

$$\mathbb{E}[\hat{E}_{\mathrm{c},\,k}] = \mathbb{E}\left[E_{\mathrm{c},\,k} + \Delta s \sum_{i=1}^{k} r_i\eta_{\mathrm{p},\,i}^{-1}\right] = E_{\mathrm{c},\,k}, \tag{46}$$

$$\begin{aligned}\mathrm{Var}[\hat{E}_{\mathrm{c},\,k}] &= \mathrm{Var}\left[\Delta s \sum_{i=1}^{k} r_i\eta_{\mathrm{p},\,i}^{-1}\right] \\ &= (\Delta s)^2 \sum_{i=1}^{k} \eta_{\mathrm{p},\,i}^{-2}\mathrm{Var}[r_\mathrm{i}] \\ &= (\Delta s)^2 \sum_{i=1}^{k} \eta_{\mathrm{p},\,i}^{-2}\sigma_{\mathrm{p},\,i}^2.\end{aligned} \tag{47}$$

In particular, the consumed energy converges to a normal distribution under the CLT, provided that the consumed energy is the sum of identically distributed random variables. In addition, under the circumstance of constant propulsion efficiency and variance, it can be concluded that the uncertainty, expressed in terms of standard deviation (STD), grows linearly with the square root of the number of unit steps k,

$$\sigma_{\hat{E}_{\mathrm{c},k}} = \frac{\Delta s\sigma_\mathrm{p}}{\eta_\mathrm{p}}\sqrt{k}. \tag{48}$$

Building on the same methods and premises, the regenerative braking energy estimate $\hat{E}_\mathrm{rb}$ can be expressed as a stochastic variable with mean and variance,

$$\mathbb{E}[\hat{E}_{\mathrm{rb},\,k}] = E_{\mathrm{rb},\,k}, \tag{49}$$

$$\mathrm{Var}[\hat{E}_{\mathrm{rb},\,k}] = (\Delta s)^2 \sum_{i=1}^{k} \eta_{\mathrm{rb},\,i}^2\sigma_{\mathrm{b},\,i}^2, \tag{50}$$

where $\eta_{\mathrm{rb},\,i}$ is the regenerative breaking efficiency and $\sigma_{\mathrm{b},\,i}^2$ is the variance of the break force esimate.

IV. Algorithm Analysis

In Section II and III, the motion model, measurement model, and CRTSS algorithm were introduced, completing the observer. In the coming Section, the observer is evaluated concerning observability, Section IV-A, and clues to the underlying structure of the observer are identified when the Kalman gain is analyzed in Section IV-B.

A. Observability

Having described the EDP in detail, the observer remains to be investigated concerning observability. In general, a system is said to be observable provided that all the states, at all times, can be estimated from only the system output. On the contrary, an unobservable system has multiple state trajectories coupled with a single output. For a nonlinear autonomous system, $\dot{\boldsymbol{x}} = \boldsymbol{f}(\boldsymbol{x})$, $y = \boldsymbol{h}(\boldsymbol{x})$, assessing the observability involves calculating the n:th Lie derivative [27],

$$\mathcal{L}_f^n\boldsymbol{h}(\boldsymbol{x}) = \frac{\partial\mathcal{L}_f^{n-1}\boldsymbol{h}(\boldsymbol{x})}{\partial\boldsymbol{x}}\boldsymbol{f}(\boldsymbol{x}), \tag{51}$$

where the first lie derivative, $\mathcal{L}_f^0\boldsymbol{h}(\boldsymbol{x}) = \boldsymbol{h}(\boldsymbol{x})$, is the measurement model. Following the Lie derivatives, the observability matrix [28],

$$\mathcal{O} = \frac{\partial}{\partial\boldsymbol{x}}\left[\mathcal{L}_f^0\boldsymbol{h}(\boldsymbol{x}) \cdots \mathcal{L}_f^n\boldsymbol{h}(\boldsymbol{x})\right]^\top, \tag{52}$$

This article has been accepted for inclusion in a future issue of this journal. Content is final as presented, with the exception of pagination.

TABLE I
PARAMETER VALUES USED WHEN DETERMINING OBSERVABILITY

Parameter	Value	Description	Unit
m	40 000	GCW	kg
ρ	1.29	Air density	$\mathrm{kg\,m^{-3}}$
θ	0	Road grade	rad
h	0	Elevation	m
T_a	0	Ambient air temperature	°C

is the Jacobian of the vertically stacked n Lie derivatives, which guarantee observability provided it is of full rank. The number of lie derivatives required to guarantee observability is at least the number of states, but possibly larger than that.

The EDP presented in this paper is, however, not an autonomous system, it is a system on the form $\dot{\boldsymbol{x}} = \boldsymbol{f}(\boldsymbol{x}, \boldsymbol{u})$, $y = \boldsymbol{h}(\boldsymbol{x})$, i.e., the observability of the system depends on the inputs. This can be addressed by treating the inputs as constant model parameters, $\boldsymbol{u} = \boldsymbol{u}_0$, and analyzing the observability around the stationary input. Using the stationary parameter values from Table I, a sweep along the states $\begin{bmatrix} v_x & T_\mathrm{t} & F_\mathrm{t} \end{bmatrix}$ give rise to the conclusion that the system is observable for all positive vehicle speeds excluding zero, and that the tire temperature and traction force had no impact on the observability. In addition, two more singularities were identified, $v_{\mathrm{w}x} = v_x$ and $v_{\mathrm{w}y} = 0$, implying that the model might lose observability under the circumstance of no side wind and when the tailwind is equal to the vehicle speed. It is important to note that the system itself does not become singular under these conditions and that the singularities in the Lie derivatives do not guarantee that the system has lost observability. Considering this, they can be avoided by adding a small term to the attack angle and the tailwind component. However, that method was disregarded as the EDP behaved effectively for almost all transport operations that the EDP was exposed to in Section V-A without addressing these singularities. Conversely, the singularity, $v_x = 0$, is troublesome, requiring adjustments to the smoothing algorithm for the EDP to function.

To avoid the singularity and incorporate the information into the smoother, the sigma points, introduced in Section III-A, are truncated at $\bar{v}_x = 1\ \mathrm{m/s^{-1}}$. The specific value chosen is not of importance, albeit it should be small enough not to have a significant impact on the kinetic energy loss $\frac{mv_x^2}{2}$. For instance, a heavy truck with a GCW of 36 tonnes exerts $\frac{1}{200}$ kWh of braking energy when making a standstill starting at 1 $\mathrm{m/s^{-1}}$. Hence, 200 stops of the same character amount to 1 kWh of energy that is not modeled by the smoother, which is a manageable size of error. Moreover, the truncation of motion calls for adjustments of the other states, specifically the traction force. Whilst the other states are on hold, the traction force,

$$F_\mathrm{t} = F_\mathrm{mr} + \frac{m(\bar{v}_x^2 - v_x^2)}{2\Delta s}, \tag{53}$$

is set to the sum of the motion resistances and the force necessary to make a constant deceleration from v_x to $1\,\mathrm{m\,s^{-1}}$. In addition, each vehicle speed sigma point is also truncated at $1\,\mathrm{m\,s^{-1}}$ before being propagated through the motion model.

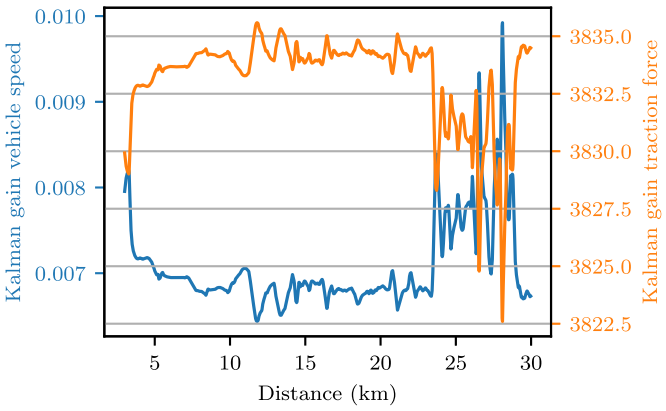

Fig. 3. The figure shows the stationary Kalman gain over a segment of a transport mission.

These adjustments are only relevant in the event of a traffic control device, characterized by its relatively short stop-time, having a negligible impact on the tire temperature.

In contrast, mission stops are often of significant duration and must therefore be modeled correctly due to their impact on the tire temperature, and consequently the rolling resistance coefficient. A switching algorithm is therefore implemented, simulating the tire temperature as a function of time, equation (4), until the stop time ends and motion resumes. During the stop time, the other states are on hold as they are all independent of time when $v_x = 0$.

B. Kalman Gain Analysis

To provide an understanding of the previously described model, it shall be connected to existing research, industry-standard definitions, and well-established theories. One common categorization of energy consumption simulation models is based on causality [29], commonly referred to as backward (inverse-dynamic) and forward (dynamic) simulations. The difference is unveiled through what is calculated and what is prescribed. In the case of a backward simulation model, the velocity is prescribed, and the forces can hence be calculated. In contrast, the forward simulation scheme calculates the forces dynamically and the vehicle motion is subsequently derived.

Upon initial inspection, the connection to the model presented in this paper is non-trivial, since the EDP presented is an observer as opposed to a simulation model. However, by reducing the intrinsic observer equations presented in Section III-A, the observer can be described by the continuous-time Luenberger observer:

$$\frac{\mathrm{d}}{\mathrm{d}s}\hat{\boldsymbol{x}} = \boldsymbol{f}(\hat{\boldsymbol{x}}, \boldsymbol{u}) + \mathbf{K}(\boldsymbol{y} - \boldsymbol{h}(\hat{\boldsymbol{x}})). \tag{54}$$

By this, it becomes clear that an observer with zero Kalman gain is equivalent to a dynamic simulation model. It may therefore be worthwhile to investigate some of the Kalman gains to further understand how the system functions.

In Figure 3, the Kalman gain over a small segment of a transport operation is presented. In particular, two Kalman

This article has been accepted for inclusion in a future issue of this journal. Content is final as presented, with the exception of pagination.

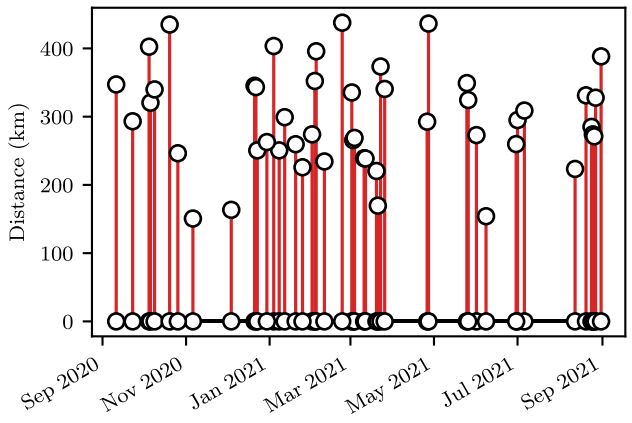

Fig. 4. The Figure shows the total travel distance covered in each of the studied transport operations.

TABLE II
A LIST OF ALL INPUT AND MEASUREMENT DATA USED BY THE EDP

Data	Variable	Source	Unit
Ambient Temperature	T_a	SMHI [2]	°C
Wind velocity	$\boldsymbol{v}_\mathrm{w}$	SMHI[2]	$\mathrm{m\,s^{-1}}$
Elevation	h	Here[3]	m
Vehicle heading angle	ϕ	Here[3]	rad
Speed limit	–	Here[3]	$\mathrm{m\,s^{-1}}$
Curvature	C	Here[3]	$\mathrm{m^{-1}}$
Traffic control devices	–	Here[3]	–
Vehicle combination	–	Log data	–
Gross combined weight	m	Log data	kg
Mission stops	–	Log data	–

gains are presented, affecting the evolution of the states v_x and F_t, respectively. Clearly, the traction force state estimate is significantly more amplified compared to the velocity state. For a unit innovation, the resulting velocity increment is 0.007 $\mathrm{m/s^{-1}}$ while the traction force increases by 3.8 kN, indicating a measurement dependence on the traction force and a motion-model dependence on the velocity state. It may thus be concluded that the EDP is a mix of a dynamic longitudinal vehicle simulation model and a statistical model, and that in stationary conditions, the EDP behaves similarly, but not equally, to a dynamic simulation model.

V. RESULT

Building on the methodology that conveys the EDP, the present Section examines the performance of the model, comparing it against vehicle log data and a benchmark model. In particular, the log data considered in this paper is collected from regular operation of a single 4×8 rigid Volvo FH truck mainly operating in Västra Götaland, Sweden, transporting up to 40 metric tonnes of gravel to the depots. The type of operation conducted includes urban delivery, regional distribution, and long haul, consequently demanding a generalized

[2]Swedish Meteorological and Hydrological Institute (SMHI), "Swedish Meteorological and Hydrological Institute (SMHI)." [Online]. Available: https://www.smhi.se

[3]"HERE Technologies." Accessed: Apr. 06, 2025. [Online]. Available: https://www.here.com

TABLE III
A LIST OF ALL THE PARAMETERS USED BY THE EDP

Parameter	Value	Unit	Description
c_1	4.09	–	C_rr at high speed[4]
c_2	19.3	–	C_rr at 0 °C [4]
A_f	10.4	$\mathrm{m^2}$	Frontal area
A_rs	13	$\mathrm{m^2}$	Rigid truck side area
A_ts	12	$\mathrm{m^2}$	Trailer side area
R_d	287	$\mathrm{J\,kg^{-1}\,K^{-1}}$	Dry air specific gas constant
R_v	461	$\mathrm{J\,kg^{-1}\,K^{-1}}$	Water vapor specific gas constant
C_0	0.6	–	Nominal air drag coefficient
φ	0	$\mathrm{s^{-1}}$	Road grade forgetting factor
Δs	25	m	Sample distance
a_yl	2	$\mathrm{m\,s^{-2}}$	Lateral acceleration limit
a_xl	1	$\mathrm{m\,s^{-2}}$	Longitudinal acceleration limit
η_p	0.67	–	Propulsion efficiency
η_b	0	–	Regenerative brake efficiency
p_d	101	kPa	Dry air pressure
p_v	0	kPa	Vapor pressure
K_p	4000	$\mathrm{N\,s\,m^{-1}}$	Proportinal gain
σ_h	0.001	m	$y_{h,\,k}$ STD
σ_v	2	$\mathrm{m\,s^{-1}}$	$y_{v,\,k}$ STD
σ_θ	0.02	$\mathrm{rad\,m^{-1}}$	$\frac{\mathrm{d}\theta}{\mathrm{d}s}$ STD
σ_{T_t}	0.04	$\mathrm{°C\,m^{-1}}$	$\frac{\mathrm{d}T_\mathrm{t}}{\mathrm{d}s}$ STD
σ_{F_t}	8200	$\mathrm{N\,m^{-1}}$	$\frac{\mathrm{d}F_\mathrm{t}}{\mathrm{d}s}$ STD

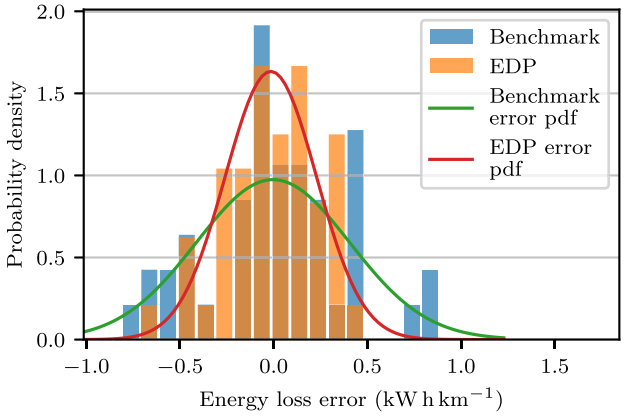

Fig. 5. The Figure is composed of two histograms, the EDP error (blue) and the benchmark error (orange), both normalized by the total distance. The model performance is indicated by the variance of the normal distributions that are fitted to each of the histograms.

EDP. In addition, the operating conditions, characterized by the weather, road, and mission specifications, vary significantly. The variation has its origin in the data logging process, which was conducted during one year, resulting in an almost uniformly distributed dataset concerning time, capturing seasonal effects on the energy consumption. These effects are manifested through a direct dependence on weather conditions and potentially also indirectly through route selection, GCW, and driver characteristics, as the haulage, driver, and customer make conscious decisions concerning the transport operation. Moreover, the transport operation exhibits daily variation both in terms of the route, cargo weight, and vehicle combination, as the driver can attach a small trailer to increase the maximum payload. Without going further into the details, the input data and data sources utilized by the EDP are listed in Table II. In Figure 4, a timeline of all transport operations considered is

This article has been accepted for inclusion in a future issue of this journal. Content is final as presented, with the exception of pagination.

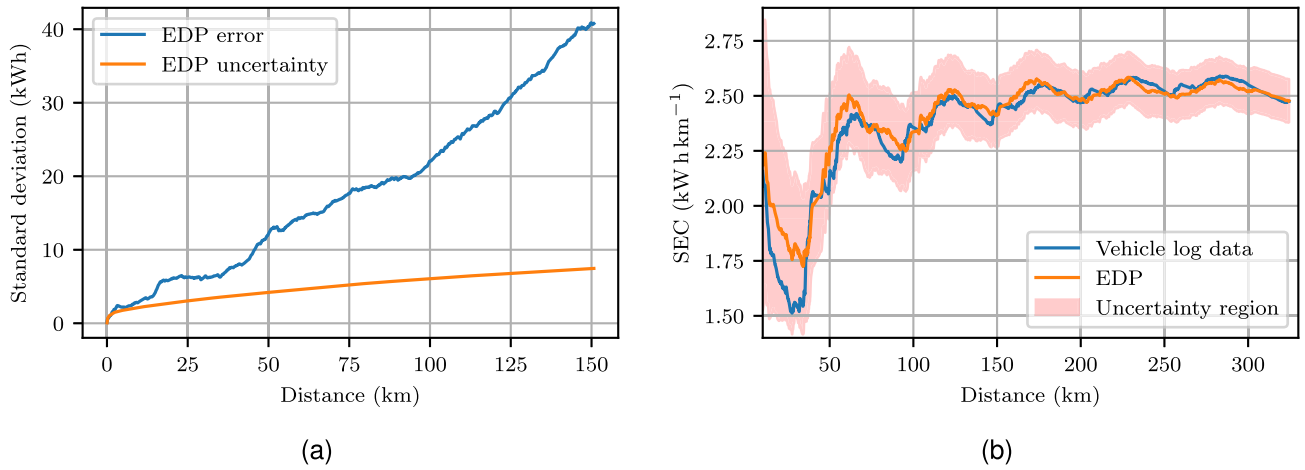

Fig. 6. In Figure (a), the error STD of EDP (blue) and the predicted uncertainty (orange) are presented. In Figure (b), the SEC value along a transport operation is displayed. Both the log data (blue) and the EDP (orange) both appear to converge as travel distance increases. The filled region represents the 3σ uncertainty region computed by the EDP.

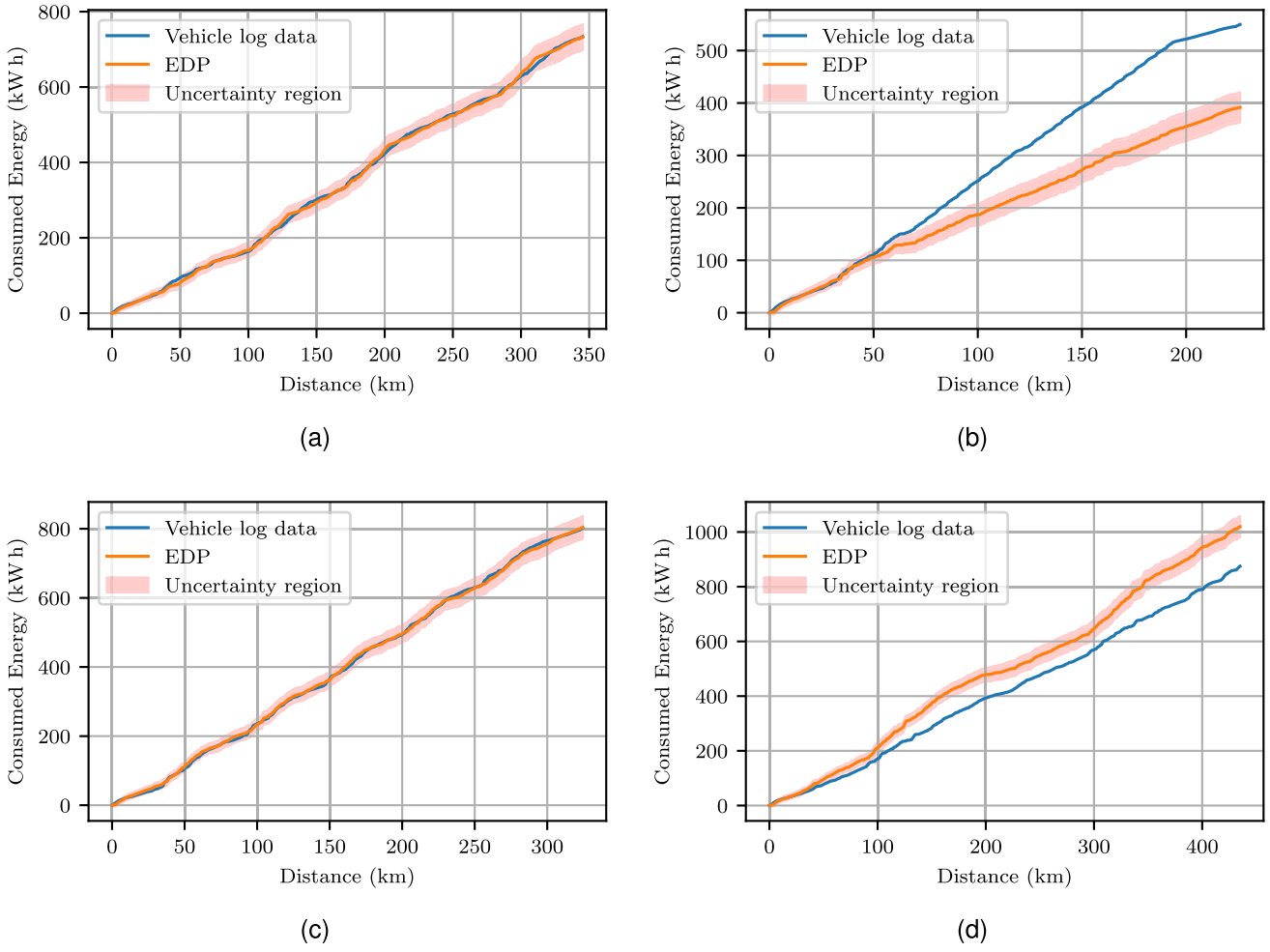

Fig. 7. The Figure compares the energy consumption logged by the vehicle (blue) and the EDP estimate (orange). The corresponding 99.7% uncertainty region is the filled area surrounding the estimate. Among all the transport operations studied, Figure (a) and (c) represent the two best predictions concerning RMSE, and Figure (b) and (d) the two worst.

presented with the total distance marked on the vertical axis. Notably, the daily variation in travel distance covered in two consecutive transport operations may differ by up to a factor of two.

This article has been accepted for inclusion in a future issue of this journal. Content is final as presented, with the exception of pagination.

Beyond the data, the model requires initialization of its states at defined values to operate correctly. For the coming case study, the vehicle speed is set to 1 m/s^{-1}, the tire temperature is the ambient temperature, and the elevation corresponds to the starting elevation above sea level. Road grade and traction force are both initialized at zero. It is especially important to carefully initialize the energy-storing states, such as the vehicle speed, to ensure an accurate EDP. Another important aspect are the model parameters, presented in Table III. Instead of deriving those from tests such as the coast-down test, standard values were adopted, owing to confidentiality reasons and limited resources. The parameters were slightly tuned to match vehicle log data and remained identical between all transport missions. Hence, the exact potential of the EDP cannot be determined, and the results presented may have been more accurate provided a better parameter setting had been adopted.

A. Case Study

To verify the EDP, it is first compared against a benchmark model concerning its mean prediction. This part merely serves as verification of the model, and may hence be performed against the most rudimentary benchmark model, the factor model. After the verification, the study addresses its ultimate objective of uncertainty estimation by comparing it against vehicle log data.

The factor model postulates that the previous transport operation's SEC, $\bar{E}_i$, and the distance, d_i, are good indicators of the current transport operation's energy demand. Using this model, the energy demand may be predicted as follows:

$$E_i = \bar{E}_{i-1} d_i. \tag{55}$$

To compare the performance of the two models in terms of their first moment, the difference between the models and the logged energy consumption is calculated. The resulting histogram is presented in Figure 5, where the variance of the *probability density function* (pdf) indicates the variation in the model error, and the mean indicates the model bias. Thus, a model with zero mean and variance has predicted the outcome perfectly, assuming that the measured energy consumption is the true energy consumption. As the means of the two models are both approximately zero, their performance is only indicated by the variance of the pdfs. Since the variance of the EDP $\sigma^2_{\text{EDP}} = 0.06$ is significantly smaller than the benchmark's $\sigma^2_{\text{B}} = 0.17$, the model prediction is verified to be sufficiently accurate.

To evaluate the uncertainty prediction, it is important to acknowledge that each transport operation is of different length, as that was shown to have a significant effect on the uncertainty in Section III-B. Hence, it is only relevant to study the uncertainty up until the total travel distance of the shortest transport operation, which in this study is approximately 150 km. In Figure 6a, the uncertainty predicted by the EDP indeed follows the behavior derived, increasing with the square root of travel distance. However, the error STD behaves linearly with the travel distance, indicating that there is still more to be modeled or that the inputs are biased. In 6a, a transport operation is analyzed concerning the SEC of the EDP and the log data, which both show signs of convergence, i.e, the variation in SEC decreases with travel distance for the EDP and the log data. Thus, the linear trend indicated by the error variance in Figure 6a contradicts the observed behavior of the logged energy consumption and the EDP.

To further investigate this, four transport operations are selected based on their root mean squared error (RMSE): the two with the smallest RMSE, Figure 7a and 7c, the one with the highest RMSE, Figure 7c, and the one with the lowest signed RMSE, Figure 7d. These transport operations are all edge cases of the complete batch, which should give insight into the linearly increasing uncertainty previously observed. Starting with the two transport operations in which the EDP performed the best, the logged energy consumption is well inside the uncertainty region, indicated by the filled area. However, analyzing the transport operations for which the EDP has the highest and lowest signed RMSE, the predicted energy consumption diverges from the logged energy consumption. In Figure 7c, the divergence occurs between 50 to 180 km and in Figure 7c, the predicted energy consumption follows the logged energy consumption apart from the region between 100 to 180 km, in which the EDP diverges from the log. Unfortunately, even though the remainder of the energy consumption is calculated with moderate precision, the divergence identified at the beginning of the transport operation is affecting the succeeding road segments, both in terms of their predicted mean and the calculated error variance presented in Figure 6a.

It shall also be noted that the STD considers all uncertainties present in real operations, including traffic, wind, temperature, driver behavior, road pavement, and more. In contrast, the EDP model merely considers reference speed variations, minor elevation measurement noise, and motion model uncertainties. Because several uncertainties are not accounted for, it is natural that the uncertainty estimate is significantly smaller than the STD. The model's full capability may therefore only be assessed once all those uncertainty sources are included.

VI. Conclusion

This study set out to model the first and second moments of energy consumption in the scenario for which the route is known, but varying between each transport operation. With inspiration from longitudinal simulation models and statistical methods, an EDP model was developed with a balance of analytical traceability, accuracy, and computational time in mind. In particular, the problem has been addressed by regarding the driver reference speed as a measurement using the CRTSS algorithm.

In Section IV-A, the EDP was analyzed concerning its observability, finding three points at which the model is potentially unobservable. These singularities guided the further development of the model, avoiding the singularities by incorporating the information into the sigma point generation and the motion model. In Section IV-B, the model was analyzed concerning its characteristics, and the conclusion was drawn that the EDP has joint features with the dynamic simulation model, but also with statistical models.

This article has been accepted for inclusion in a future issue of this journal. Content is final as presented, with the exception of pagination.

In V-A, the first and second moments of energy consumption were analyzed and compared against log data and a benchmark model. The results showed a promising outlook, in which the first moment was significantly better predicted by the EDP compared to the benchmark model. Moreover, the second moment of energy consumption was predicted and subsequently compared against log data. In the comparison, the EDP model error STD was found to grow linearly with distance, contradicting the estimated uncertainty of the EDP. However, after investigating a set of transport operations, it was concluded that the linear growth in the error STD could be attributed to input bias and unmodeled processes. In particular, considering traffic density and other vehicle speed-related road data could potentially prove effective. In addition, the inclusion of more supplementary states, e.g., wind velocity and temperature, and a rigorous investigation on the off-diagonal elements of the process noise covariance matrix should increase the accuracy of the uncertainty. Moreover, a detailed description of the drivetrain could have a significant effect on the accuracy of the first and second moments, as the imposed drivetrain of the EDP utilizes a constant efficiency.

In the end, the results indicate that the model is able to predict the energy demand well for the given experimental setup: driver, vehicle, and operating conditions considered in this study. Still, further validation in another setting shall be conducted to corroborate the general effectiveness of the proposed EDP.

REFERENCES

[1] *Global Ev Outlook* 2025, International Energy Agency, Paris, France, 2023.

[2] *Report of the Swedish Climate Policy Council*, Swedish Climate Policy Council, Stockholm, Sweden, Mar. 2021.

[3] Regulation (EU) 2019/*1242 of the European Parliament and of the Council*, European Parliament and Council, Brussels, Belgium, 2019.

[4] R. Al-Dal'ain and D. Celebi, "Planning a mixed fleet of electric and conventional vehicles for urban freight with routing and replacement considerations," *Sustain. Cities Soc.*, vol. 73, Oct. 2021, Art. no. 103105.

[5] R. Basso, B. Kulcsár, B. Egardt, P. Lindroth, and I. Sanchez-Diaz, "Energy consumption estimation integrated into the electric vehicle routing problem," *Transp. Res. D, Transp. Environ.*, vol. 69, pp. 141–167, Apr. 2019.

[6] E. Demir, T. Bektaş, and G. Laporte, "A review of recent research on green road freight transportation," *Eur. J. Oper. Res.*, vol. 237, no. 3, pp. 775–793, Sep. 2014.

[7] U. S. E. P. Agency. (2012). *Motor* Vehicle Emission Simulator (Moves): User's Guide for Moves2010b. [Online]. Available: https://www.epa.gov/oms/models/moves/documents/420b12001b.pdf

[8] N. A. E. Inventory. (2012). *Emission Factors*. [Online]. Available: https://naei.defra.gov.uk/data/emission-factors

[9] *NTMCalc Basic*, Network for Transport Measures (NTM), Stockholm, Sweden. [Online]. Available: https://www.transportmeasures.org/ntmcalc/v4/basic/index.html#/

[10] P. Good and J. Hardin, *Common Errors in Statistics (and How to Avoid Them)*, 3rd ed., Hoboken, NJ, USA: Wiley, 2009.

[11] M. Lin, S. Chen, J. Meng, W. Wang, and J. Wu, "Instantaneous energy consumption estimation for electric buses with a multi-model fusion method," *IEEE Trans. Intell. Transp. Syst.*, vol. 26, no. 1, pp. 371–381, Jan. 2025.

[12] J. Bi, Y. Wang, S. Shao, and Y. Cheng, "Residual range estimation for battery electric vehicle based on radial basis function neural network," *Measurement*, vol. 128, pp. 197–203, Nov. 2018, doi: 10.1016/j.measurement.2018.06.054.

[13] C. Emvin, F. Bruzelius, L. Romano, B. Jacobson, P. Johannesson, and R. Andersson, "A propulsion energy estimator for road vehicles," in *Proc. Adv. Vehicle Control Symp.*, Oct. 2024, pp. 315–321.

[14] D. Li, Q. Hu, W. Jiang, H. Dong, and Z. Song, "Integrated power and thermal management for enhancing energy efficiency and battery life in connected and automated electric vehicles," *Appl. Energy*, vol. 396, Oct. 2025, Art. no. 126213. [Online]. Available: https://www.sciencedirect.com/science/article/pii/S0306261925009432

[15] R. Basso, B. Kulcsár, and I. Sanchez-Diaz, "Electric vehicle routing problem with machine learning for energy prediction," *Transp. Res. B, Methodol.*, vol. 145, pp. 24–55, Mar. 2021.

[16] S. Sautermeister, M. Falk, B. Bäker, F. Gauterin, and M. Vaillant, "Influence of measurement and prediction uncertainties on range estimation for electric vehicles," *IEEE Trans. Intell. Transp. Syst.*, vol. 19, no. 8, pp. 2615–2626, Aug. 2018.

[17] C. Fiori, V. Marzano, V. Punzo, and M. Montanino, "Energy consumption modeling in presence of uncertainty," *IEEE Trans. Intell. Transp. Syst.*, vol. 22, no. 10, pp. 6330–6341, Oct. 2021.

[18] A. T. Thorgeirsson, S. Scheubner, S. Funfgeld, and F. Gauterin, "Probabilistic prediction of energy demand and driving range for electric vehicles with federated learning," *IEEE Open J. Veh. Technol.*, vol. 2, pp. 151–161, 2021.

[19] A. T. Thorgeirsson and F. Gauterin, "Probabilistic predictions with federated learning," *Entropy*, vol. 23, no. 1, pp. 1–13, Dec. 2020.

[20] C.-M. Tseng and C.-K. Chau, "Personalized prediction of vehicle energy consumption based on participatory sensing," *IEEE Trans. Intell. Transp. Syst.*, vol. 18, no. 11, pp. 3103–3113, Nov. 2017.

[21] L. Ydrefors, M. Hjort, S. Kharrazi, J. Jerrelind, and A. S. Trigell, "Rolling resistance and its relation to operating conditions: A literature review," *Proc. Inst. Mech. Engineers, D, J. Automobile Eng.*, vol. 235, no. 12, pp. 2931–2948, Oct. 2021, doi: 10.1177/09544070211011089.

[22] J. Hyttinen, M. Ussner, R. Österlöf, J. Jerrelind, and L. Drugge, "Truck tyre transient rolling resistance and temperature at varying vehicle velocities–measurements and simulations," *Polym. Test.*, vol. 122, May 2023, Art. no. 108004.

[23] M. Askerdal, J. Fredriksson, and L. Laine, "Development of simplified air drag models including crosswinds for commercial heavy vehicle combinations," *Vehicle Syst. Dyn.*, vol. 62, no. 5, pp. 1085–1102, May 2024, doi: 10.1080/00423114.2023.2213786.

[24] L. Romano, K. Podgórski, C. Emvin, P. Johannesson, J. Fredriksson, and F. Bruzelius, "A stochastic theory of longitudinal dynamics and energy consumption of road vehicles," *IEEE Trans. Intell. Vehicles*, vol. 10, no. 3, pp. 1–21, Mar. 2025.

[25] P. Pettersson, S. Berglund, B. Jacobson, L. Fast, P. Johannesson, and F. Santandrea, "A proposal for an operating cycle description format for road transport missions," *Eur. Transp. Res. Rev.*, vol. 10, no. 2, pp. 1–19, Jun. 2018.

[26] S. Särkkä, *Bayesian Filtering and Smoothing*, vol. 3. Cambridge, U.K.: Cambridge Univ. Press, 2013. [Online]. Available: https://users.aalto.fi/~ssarkka/pub/cup_book_online_20131111.pdf

[27] H. Khalil, *Nonlinear Systems*, 3rd ed., London, U.K.: Pearson, 2014.

[28] R. Hermann and A. J. Krener, "Nonlinear controllability and observability," *IEEE Trans. Autom. Control*, vol. AC-22, no. 5, pp. 728–740, Oct. 1977.

[29] P. Pettersson, B. Jacobson, F. Bruzelius, P. Johannesson, and L. Fast, "Intrinsic differences between backward and forward vehicle simulation models," *IFAC-PapersOnLine*, vol. 53, no. 2, pp. 14292–14299, 2020.

Carl Emvin received the M.Sc. degree in systems, control and mechatronics from the Chalmers University of Technology, Gothenburg, Sweden, in 2023, where he is currently pursuing the Ph.D. degree with the Vehicle Dynamics Research Group, Department of Mechanics and Maritime Sciences. During his studies and internship with Volvo Trucks, he became proficient in using and developing longitudinal vehicle simulation models. During his master's thesis project, he contributed to the operating cycle format, a collection of stochastic processes that describe vehicle use. His research focuses on energy demand predictions, closely connected with energy consumption, and residual range estimation.

This article has been accepted for inclusion in a future issue of this journal. Content is final as presented, with the exception of pagination.

Luigi Romano (Member, IEEE) received the M.Sc. degree in mechanical engineering from the University of Naples "Federico II," Italy, in 2018, the Ph.D. degree in vehicle engineering from the Chalmers University of Technology, Gothenburg, Sweden, in 2023, and the second M.Sc. degree in applied mathematics from the University of Gothenburg. Since 2024, he has been affiliated with the Vehicular Systems Group, Department of Electrical Engineering, Linköping University, where he is a VR Post-Doctoral Fellow funded by Swedish Research Council. His primary research interests include the mathematical modeling and analysis of vehicular systems and components, with particular emphasis on pure road vehicle dynamics and energy-related aspects, as well as the development of control and estimation algorithms for automotive and transportation applications.

Fredrik Bruzelius received the M.Sc. degree in applied mathematics from Linköping University in 1999, and the Ph.D. degree in automatic control and the Docent degree in vehicle dynamics from the Chalmers University of Technology, in 2004 and 2014, respectively. He is currently a Senior Researcher in vehicle dynamics with the Department of Mechanics and Maritime Sciences, Chalmers University of Technology. He has a broad interests in vehicle dynamics estimation and control.

Bengt Jacobson received the Ph.D. degree in machine elements from the Chalmers University of Technology, Sweden, in 1993, studying the dynamics of gear shifting in power-shifting transmissions. He continued research on longitudinal vehicle dynamics with dynamic modeling and control of powertrain systems, including hybrid vehicles. Based on this topic and teaching in vehicle dynamics, he was entitled as an Associate Professor in 1998. He was a Technical Expert (2001–2010) with Volvo Car Corporation with a focus on vehicle dynamics control and active safety, mainly focusing on brakes and steering. He is currently a Professor and a Group Leader of Vehicle Dynamics Group, Chalmers University of Technology.

Rickard Andersson received the M.Sc. degree from the Department of Physics University of Gothenburg in 1996. He has been with Volvo since 2005 and is currently a Leader in the simulation and data science area. Since then, he has worked in many positions within automotive and aerospace companies. At Volvo, he gained deep experience from system simulation modeling with an energy prediction focus. He has held several positions in Swedish research foundations and EU projects. He is currently the Project Leader of the U-FEEL Project, founded by Swedish Energy Authority (FFI frame), managing customer operation research with the objective of reducing CO_2 emissions.

Pär Johannesson received the Ph.D. degree in mathematical statistics from Lund Institute of Technology, Lund, Sweden, in 1999, with a thesis on statistical load analysis for fatigue. He has a postdoctoral position in mathematical statistics with the Chalmers University of Technology and PSA Peugeot Citroën in France. He is also a Docent in mathematical statistics at the Chalmers University of Technology. He is currently a Senior Researcher in mechanical reliability, fatigue, and load analysis with the RISE Research Institutes of Sweden, Gothenburg, Sweden. He has more than 30 years of experience in research and development in fatigue and load analysis with a focus on engineering statistics and reliability in industrial applications. He has published more than 25 articles in international journals. He is a Co-Editor of the handbook *Guide to Load Analysis for Durability in Vehicle Engineering*.